Journal of Computational Physics 229 (2010) 4522–4543

Contents lists available at ScienceDirect

Journal of Computational Physics

journal homepage: www.elsevier.com/locate/jcp

Behavior of viscous solutions in Lagrangian formulation

Zhijun Shen *, Wei Yan *, Guixia Lv *

Laboratory of Computational Physics, Institute of Applied Physics and Computational Mathematics, P.O. Box 8009-26, Beijing 100088, China

ARTICLE INFO

Article history:
Received 21 August 2009
Received in revised form 23 February 2010
Accepted 24 February 2010
Available online 1 March 2010

Keywords:
Lagrangian coordinate
Fluid hydrodynamics
Overheating
Viscosity

ABSTRACT

In this paper, the behavior of shock-capturing methods in Lagrangian coordinate is investigated. The relation between viscous shock and inviscid one is analyzed quantitatively, and the procedure of a viscous shock formation and propagation with a jump type initial data is described. In general, a viscous shock profile and a discontinuous one include different energy and momentum, and these discrepancies result in the generation of waves in all families when a single wave Riemann problem (shock or rarefaction) is solved. Employing this method, some anomalous behavior, such as, viscous shock interaction, shock passing through ununiform grids, postshock oscillations and lower density phenomenon is explained well. Using some classical schemes to solve the inviscid flow in Lagrangian coordinate may be not adequate enough to correctly describe flow motion in the discretized space. Partial discrepancies between von Neumann artificial viscosity method and Godunov method are exhibited. Some reviews are given to those methods which can ameliorate even eliminate entropy errors. A hybrid scheme based on the understanding to the behavior of viscous solution is proposed to suppress the overheating error.

1. Introduction

In the past few decades remarkable progress has been made in the development of numerical methods for solving the inviscid flow equations. Among many methods two classical schemes for shock capturing are widely used. The first is artificial viscosity method proposed by von Neumann and Richtmyer [1]; they added sufficient artificial viscosity in the governing equations to produce shock structures which could be resolved on the scale of the cell size. The second is the Godunov method [2] which introduces a discontinuity at the cell interface and the Riemann solution is used for the flux evaluation, followed by the cell average to construct constant states inside each cell.

These two types of schemes are often robust and accurate, however, they can on occasions fail quite spectrally, such as have startup error, the postshock oscillation, shock instability and wall heating (overheating) phenomenon. In an important paper, Quirk catalogued a number of situations in which anomalous behavior was known to occur [3] and some papers have been proposed to explain these phenomena. For example for the postshock oscillations, Roberts found an error consisting of a long wavelength noise in the downstream running wave families. This error is not effectively damped by the dissipation of the scheme and may contribute to the slow convergence to steady state case[4]. Jin and Liu explained the postshock oscillations in the context of traveling wave solution and suggested that the momentum spike was the cause for the oscillations [5]. Karni and Canic regarded that the small viscosity in Roe's scheme at the shock region contributes to the oscillations, and derived a parabolic modified equation plus a small perturbation in the shock layer [6]. Arora and Roe interpreted it as that the intermediate states inside the shock layer did not lie on the Hugoniot curve [7]. Hence, the Riemann solver generated a whole fan of waves and induced the postshock oscillations. Kun Xu and Jishan Hu ascribed the oscillations to dynamical

* Corresponding authors. Tel.: +86 10 62014411 2956; fax: +86 10 62057289 (Z. Shen).
E-mail addresses: shen_zhijun@iapcm.ac.cn (Z. Shen), wyanmath@hotmail.com (W. Yan), lvguixia@126.com (G. Lv).

0021-9991/$ - see front matter © 2010 Elsevier Inc. All rights reserved.
doi:10.1016/j.jcp.2010.02.020

effects on the projection stage of Godunov method [8]. The unsteadiness of viscosity coefficient rather than the momentum spike was the main reason of postshock oscillations. They constructed a physical model for the dynamical averaging, derived the governing equations and quantitatively figured out the time dependent dissipative mechanism in the projection stage for the moving shock case. All of these explanations are based on Godunov method in Eulerian coordinate system, by now we have not seen similar explanation in artificial viscosity method.

Wall heating (entropy) error is another famous example, which is usually present in the problem of a strong shock reflecting from a rigid wall or at the sudden start up of a piston. Conventional schemes applied to this problem give numerical approximations with a consistent $O(1)$ error in the density and internal energy next to the wall. This problem has been studied since the dawn of simulating shock waves [9] and has been revisited many times ever since then by [10–15]. Noh [10] investigated the "excess heating error" in the context of the artificial viscosity approach. With mesh refinement he observed that the numerical difference solution was essentially unchanged with respect to the wall heating error, and especially the peak pointwise error was constant in magnitude. This experimentation leads him to conclude that the error is inevitable because it is built into the exact solution to the differential equations defining the artificial viscosity method. Similar conclusions were attained by Menikoff in [11] when he researched on viscous shock interaction; he noticed that the fronts of some conservative quantities in viscous shock were not the same and argued that the numerical error was due to the artificial shock width. His observation led him to conjecture that all shock capturing schemes without significant heat conduction would have the same type of qualitative entropy error. Rider noticed the different behavior of a wall heating phenomenon in the Lagrangian or Eulerian coordinates system. The Lagrangian solution always suffers from large overheating error near the wall for cylindrical and spherical geometry, while using the same method in Eulerian coordinates experiences this phenomenon more slightly. He offered an explanation based on phase error and grid nonuniformity [13].

It is well known that without a full understanding of the nature of a numerical phenomenon, one cannot expect to develop a robust scheme to filter out these kinds of errors very well.

The current work benefits from all previous experiences and focuses on the study of some anomalous phenomena in Lagrangian formalism, such as wall heating, postshock oscillations. We hope to use a uniform theory to explain such numerical observations. By the idea borrowed from Menikoff [11], we perform an analysis of traveling wave shock profile with von Neumann viscosity and ascribe the error to asymptotic initial shock layer when shock transforms from discontinuous data to viscous profile. The viscous solution with constant propagation velocity may include different momentum or energy with inviscid solution. These discrepancies will be described by those quantities: the relative distance, momentum, and energy between viscous shock wave and inviscid shock wave. Our method and that in [11] are different in that these quantities are defined in mass coordinate and therefore they have simpler expression than those in [11]. Our analysis is based on linear viscosity rather than quadratic viscosity in order to compare better with Godunov method. The solution with linear viscosity loses compact support shock transition zone, so it is more difficult to describe the concept of total energy and momentum of this zone. The theory are used to explain much anomalous phenomena.

The relative energy and dissipation mechanism in a numerical scheme are the source of overheating/cooling (wall heating/cooling) errors. For the problems whose relative energy can be computed exactly, the behavior of viscous solution may be forecast in some situations. But the relative energy and momentum do not result in postshock oscillations directly, the unsteadiness of viscosity term is the cause of such behavior. Just like pointed out in [7], the postshock oscillations are inevitable in numerical calculation. Moreover we think the concrete amplitude depends on the competition between magnitude of relative momentum(energy) and ability of the dissipation. Using these ideas, some anomalous numerical artifacts, such as wall heating, oscillations in shock wave interaction and in shock wave passing through nonuniform grids can be explained well. These ideas can be also extended to other viscous equations and other problems, such as Godunov type Lagrangian method and viscous rarefaction wave problem.

There are lots of numerical schemes in Godunov method regime. Instead of guessing the underlying wave equations for the "numerical fluids", we research modified equations from Godunov method based on some approximate Riemann solvers. Due to the different viscosity mechanism with artificial viscosity method, the results of the viscous shock interaction and behavior of postshock oscillations are slightly different.

Since all anomalous behavior in shock capturing schemes is due to viscosity and dissipative mechanism, decreasing the effects of viscosity and diffusing the error to the whole solution are two main methods to ameliorate such errors in computation. High resolution Godunov method can effectively ameliorate the overheating errors in rarefaction waves and shock propagation, but fail in shock collision problem. The HLL type method [16] can diffuse entropy error but suffer from itself large viscosity. For example, the entropy errors are still obvious for some rarefaction wave problems. To combine the advantages of both schemes, a simple hybrid Godunov method is proposed to suppress the overheating error.

In Section 2, the inviscid gas dynamics equations in Eulerian and Lagrangian frames are given; the viscous equations arose from artificial viscosity method and some kinds of approximate Riemann solver Godunov method are described. In Section 3 the traveling shock wave structures of different viscous equations are analyzed; the relative distance, relative momentum and relative energy established in mass coordinate are introduced. The formation and propagation process of a viscous shock with jump type initial data is described and analyzed in Section 4, and many numerical evidences are illustrated. Furthermore variable viscosity is considered in Section 5. The behavior of shock passing through ununiform grids and postshock oscillations are explained. A rarefaction wave problem is considered in Section 6. Finally some methods to ameliorate or eliminate entropy and momentum errors are reviewed and partial results are exhibited numerically. A hybrid method to deduce the entropy error is proposed in Section 7.

The calculation in artificial viscosity method of this paper is performed with the G1DE code which comes from a floppy diskette attached to book [17]. The code uses a support operator algorithm with stagger spatial and temporal step. The artificial viscosity uses constant or linear Landshoff viscosity [18]. A tiny modification to G1DE in solving isentropic equations is made. The numerical results obtained by Godunov method in this paper use exact Riemann solver except some special declarations. The algorithms for the Godunov methods in this paper are described in Appendix B.

2. Governing equations

Let's consider the gas dynamics equations for inviscid compressible fluid

$$\begin{aligned} &\rho_t + (\rho u)_x = 0, \\ &(\rho u)_t + (\rho u^2 + P)_x = 0, \\ &(\rho E)_t + (\rho E u + P u)_x = 0, \end{aligned} \tag{1}$$

where ρ, E and u denote the density, the specific total energy and the fluid velocity, respectively. We denote by $e = E - \frac{1}{2}u^2$ the specific internal energy and P the pressure given by the ideal gas equation of state (EOS) $P = (\gamma - 1)\rho e$, here γ is specific heat ratio. The eigenvalue of the Jacobian matrix in this system are $\lambda_1 = u - c$, $\lambda_2 = u$, $\lambda_3 = u + c$, where $c = \gamma p/\rho$ is sound speed. They correspond to two nonlinear acoustic waves (1-wave and 3-wave, shock or rarefaction wave) and a linear degenerate entropy wave (2-wave, contact discontinuity). The corresponding right eigenvectors are

$$r_1 = \begin{bmatrix} 1 \\ u - c \\ H - uc \end{bmatrix}, \quad r_2 = \begin{bmatrix} 1 \\ u \\ u^2/2 \end{bmatrix}, \quad r_3 = \begin{bmatrix} 1 \\ u + c \\ H + uc \end{bmatrix},$$

respectively, where the total specific enthalpy is $H = E + P/\rho$.

By introducing the Lagrangian coordinate ξ given by $\xi = \int_{x_0(t)}^{x} \rho(z,t)dz$, where $x_0(t)$ denotes the Eulerian coordinate of a given fluid particle, the Euler Eq. (1) can be transformed into Lagrangian form

$$\begin{cases} \tau_t - u_\xi = 0, \\ u_t + P_\xi = 0, \\ E_t + (Pu)_\xi = 0, \end{cases} \tag{2}$$

where $\tau = 1/\rho$ is the specific volume. When the EOS is for ideal gas, i.e., $P = (\gamma - 1)\rho e$, the Jacobin matrix of Eq. (2) [19,20] is

$$JM = \begin{bmatrix} 0 & -1 & 0 \\ -P/\tau & -(\gamma - 1)u/\tau & (\gamma - 1)/\tau \\ -Pu/\tau & P - (\gamma - 1)u^2/\tau & (\gamma - 1)u/\tau \end{bmatrix}.$$

The right eigenvectors of the Jacobin matrix are

$$r_1 = \begin{bmatrix} 1 \\ \rho c \\ \rho c u - P \end{bmatrix}, \quad r_2 = \begin{bmatrix} 1 \\ 0 \\ P/(\gamma - 1) \end{bmatrix}, \quad r_3 = \begin{bmatrix} 1 \\ -\rho c \\ -\rho c u - P \end{bmatrix}, \tag{3}$$

and the eigenvalues are $\lambda_1 = -\rho c$, $\lambda_2 = 0$, $\lambda_3 = \rho c$, respectively.

Under the assumption that the entropy is constant everywhere, Eq. (2) can be simplified into an isentropic model (p-system)

$$\begin{cases} \tau_t - u_\xi = 0, \\ u_t + P_\xi = 0, \end{cases} \tag{4}$$

where the EOS is $P = A\rho^\gamma$, A is a constant. For this 2×2 system, the nonlinear characteristic field includes two waves

$$r_1 = \begin{bmatrix} 1 \\ \rho c \end{bmatrix}, \quad r_2 = \begin{bmatrix} 1 \\ -\rho c \end{bmatrix}, \tag{5}$$

traveling with speeds which are equal to the eigenvalues $\lambda_1 = -\rho c$, $\lambda_2 = \rho c$, where the sound speed $c = \sqrt{\gamma A \rho^{\gamma - 1}}$.

In order to distinguish the Eq. (2) from (4), we call fully Euler Eq. (2) as adiabatic models or adiabatic equations disregarding strictness hereafter.

3. Numerical methods and viscous equations

3.1. Artificial viscosity method for adiabatic equations

von Neumann presented an artificial viscosity method for solving compressible adiabatic equations. The numerical method employs stagger grid in time and space to keep the discrete error in second order with following viscous equations:

$$\begin{cases} \tau_t - u_\xi = 0, \\ u_t + (P+q)_\xi = 0, \\ E_t + ((P+q)u)_\xi = 0, \end{cases} \tag{6}$$

where q is an artificial viscosity pressure in quadratic form [1]

$$q = \begin{cases} \varepsilon^2 \rho (\partial u/\partial \xi)^2, & \text{if } \partial u/\partial \xi < 0, \\ 0, & \text{others}, \end{cases}$$

or linear form [18]

$$q = \begin{cases} -\varepsilon \rho c_0 (\partial u/\partial \xi), & \text{if } \partial u/\partial \xi < 0, \\ 0, & \text{others}, \end{cases} \tag{7}$$

where ε is the viscous coefficient, c_0 is a constant adiabatic speed of sound. For both viscosity forms there exist explicit traveling shock wave solutions when ε is constant.

For a right facing shock wave U, the left and right states (after and before the shock) are

$$\begin{aligned} &\lim_{\xi \to -\infty} U(\xi, 0) = U_L = (\tau_a, u_a, P_a, E_a)^T, \\ &\lim_{\xi \to +\infty} U(\xi, 0) = U_R = (\tau_b, u_b, P_b, E_b)^T, \end{aligned} \tag{8}$$

respectively. Let s be the shock velocity in Lagrangian coordinate, then from Rankine–Hugoniot conditions there are

$$\begin{cases} u = u_a - s(\tau - \tau_a) = u_b - s(\tau - \tau_b), \\ P + q = P_a + s(u - u_a) = P_b + s(u - u_b), \\ Pu + qu = P_a u_a + s(E - E_a) = P_b u_b + s(E - E_b). \end{cases} \tag{9}$$

Here we just give a traveling shock structure for linear form viscosity, as to a quadratic viscosity form, see Appendix A. At the initial states (8), the viscous profiles of transition zone of (7) are

$$\begin{aligned} \tau &= \frac{\tau_b + \tau_a}{2} + \frac{\tau_b - \tau_a}{2} \frac{e^{a\omega} - 1}{e^{a\omega} + 1}, \\ u &= \frac{u_b + u_a}{2} + \frac{u_b - u_a}{2} \frac{e^{a\omega} - 1}{e^{a\omega} + 1}, \\ P + q &= \frac{P_b + P_a}{2} + \frac{P_b - P_a}{2} \frac{e^{a\omega} - 1}{e^{a\omega} + 1}, \\ E &= \frac{E_b + E_a}{2} + \frac{E_b - E_a}{2} \frac{e^{a\omega} - 1}{e^{a\omega} + 1} - (u_b - u_a)^2 \frac{e^{a\omega}}{(e^{a\omega} + 1)^2}, \end{aligned} \tag{10}$$

where $a = \frac{(\gamma+1)(u_a - u_b)}{2\varepsilon c_0}$, $\omega = \xi - st$.

Solution (10) shows that the linear viscosity acts throughout the flow, and the viscous shock width is infinite. Actually when ε is very small, the solution (10) approaches an inviscid shock rapidly. Define an effective shock transition zone as

$$\{\xi : |\tau(\xi) - \tau_a| \geqslant \varepsilon_0 |\tau_b - \tau_a|\} \cup \{\xi : |\tau(\xi) - \tau_b| \geqslant \varepsilon_0 |\tau_b - \tau_a|\},$$

where $\varepsilon_0 > 0$ is a small parameter. Then the effective shock width is

$$\frac{4\varepsilon c_0}{(\gamma+1) s(\tau_b - \tau_a)} \ln \frac{1 - \varepsilon_0}{\varepsilon_0}, \tag{11}$$

where the width depends on shock strength $s(\tau_b - \tau_a)$.

Similar to the idea of Menikoff [11], we define the shock positions of viscous profiles of specific volume, velocity and energy as ξ_s^τ, ξ_s^u, ξ_s^E, so that

$$\begin{aligned} &\int_{-\infty}^{\xi_s^\tau} (\tau - \tau_a) d\xi + \int_{\xi_s^\tau}^{\infty} (\tau - \tau_b) d\xi = 0, \quad \text{(i)} \\ &\int_{-\infty}^{\xi_s^u} (u - u_a) d\xi + \int_{\xi_s^u}^{\infty} (u - u_b) d\xi = 0, \quad \text{(ii)} \\ &\int_{-\infty}^{\xi_s^E} (E - E_a) d\xi + \int_{\xi_s^E}^{\infty} (E - E_b) d\xi = 0. \quad \text{(iii)} \end{aligned} \tag{12}$$

These front positions describe a shift between inviscid shock and viscous shock.

Substituting the analytical solution (10) into (12) in a moving mass coordinate system with velocity s gives

$$\xi_s^\tau = \xi_s^u = 0 > \xi_s^E = -\frac{(u_a-u_b)^2}{(E_a-E_b)a} = -\frac{2(u_a-u_b)}{(\gamma+1)(E_a-E_b)}\varepsilon c_0. \tag{13}$$

This means the front of velocity profile is the same as that of specific volume, and the energy front gets behind that of specific volume along shock propagation direction. We denote relative distance between the fronts of velocity, energy and specific volume profiles by

$$\begin{aligned}\delta_{u\tau} &= \xi_s^u - \xi_s^\tau = 0,\\ \delta_{E\tau} &= \xi_s^E - \xi_s^\tau = -\frac{2(u_a-u_b)}{(\gamma+1)(E_a-E_b)}\varepsilon c_0.\end{aligned} \tag{14}$$

Fig. 1(a) gives the velocity and energy profiles of solution (10) for the Noh problem [10]. The energy front drops behind the velocity one for the right facing shock. This is seen much more clearly in Fig. 1(b), which shows the same solution on a different scale.

Define relative momentum and energy of viscous shock between the two fronts as

$$\begin{aligned}\delta M &= \int_{-\infty}^{\xi_s^\tau}(u-u_a)d\xi + \int_{\xi_s^\tau}^{\infty}(u-u_b)d\xi,\\ \delta E &= \int_{-\infty}^{\xi_s^\tau}(E-E_a)d\xi + \int_{\xi_s^\tau}^{\infty}(E-E_b)d\xi.\end{aligned}$$

There is

$$\begin{aligned}\delta M &= \delta_{u\tau}(u_a-u_b) = 0,\\ \delta E &= \delta_{E\tau}(E_a-E_b) = -\frac{(u_a-u_b)^2}{a} = -\frac{2(u_a-u_b)}{(\gamma+1)}\varepsilon c_0.\end{aligned} \tag{15}$$

The relative energy δE depends linearly on the relative distance $\delta_{E\tau}$ and viscous coefficient ε. In addition, there are two properties for relative distance: (i) δE is a function of the shock strength, i.e., $\delta E \sim (u_b - u_a)$ for linear viscosity, $\delta E \sim (u_b-u_a)^2$ for quadratic viscosity (see Appendix A). (ii) δE is a function of the specific heat ratio.

In summary, let $V_T(U) = \int_{-\infty}^{\infty}\tau d\xi,\ M_T(U) = \int_{-\infty}^{\infty} u d\xi,\ E_T(U) = \int_{-\infty}^{\infty} E d\xi$ represent total volume, momentum and total energy of a solution $U = (\tau, u, E)$, respectively, then

Remark 1. If we define an inviscid shock U_0 at ξ_s^τ with initial discontinuous data (8), then there are

$$\begin{cases} V_T(U_0-U) = 0,\\ M_T(U_0-U) = 0,\\ E_T(U_0-U) \geqslant 0,\end{cases}$$

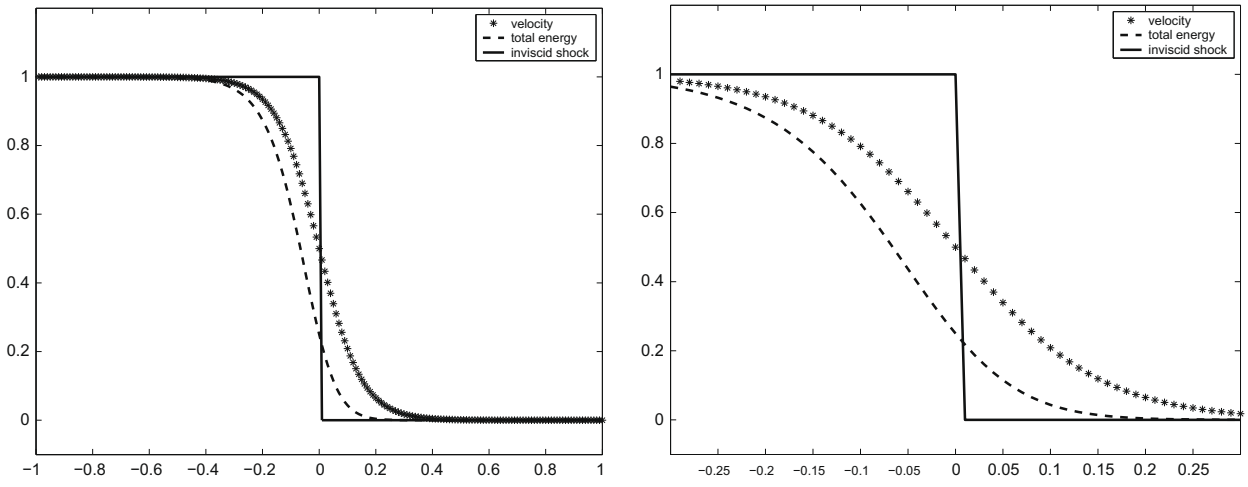

Fig. 1. Velocity and energy distribution inside shock layer from solution (10), solid line is discontinuous shock, dotted line is velocity, and dash-dotted is energy. Right is magnification of the same results.

where U is the viscous shock (10). That means, total volume and momentum of viscous shock are the same as that of U_0, but total energy of steady state shock is less than U_0.

3.2. Artificial viscosity method for isentropic equations

The numerical method for isentropic Eq. (4) is the same as (6) except energy equation. So the viscous Navier Stokes equations are

$$\begin{cases} \tau_t - u_\xi = 0, \\ u_t + (P+q)_\xi = 0, \end{cases} \tag{16}$$

in which viscosity term q has the same form as (7). In a right face traveling shock at speed s, the initial physical quantity $U = (\tau, u)^T$ satisfies

$$\begin{aligned} &\lim_{\xi\to-\infty} U(\xi,0) = U_L = (\tau_a, u_a)^T, \\ &\lim_{\xi\to+\infty} U(\xi,0) = U_R = (\tau_b, u_b)^T. \end{aligned} \tag{17}$$

Then according to Hugoniot conditions, there are

$$\begin{cases} u = u_a - s(\tau - \tau_a) = u_b - s(\tau - \tau_b), \\ P + q = P_a + s(u - u_a) = P_b + s(u - u_b). \end{cases} \tag{18}$$

This 2×2 system includes two profiles: the specific volume and velocity ones. Define the shock positions of viscous profiles of specific volume and velocity as $\xi_s^\tau,\ \xi_s^u$, where

$$\begin{aligned} &\int_{-\infty}^{\xi_s^\tau} (\tau - \tau_a)d\xi + \int_{\xi_s^\tau}^{\infty} (\tau - \tau_b)d\xi = 0, \quad \text{(i)} \\ &\int_{-\infty}^{\xi_s^u} (u - u_a)d\xi + \int_{\xi_s^u}^{\infty} (u - u_b)d\xi = 0. \quad \text{(ii)} \end{aligned} \tag{19}$$

It is unnecessary to write out the explicit solution of (16). According to Rankine–Hugoniot conditions (18), we get $\xi_s^\tau = \xi_s^u$. If we define relative distance and momentum as Section 3.1, then the relative distance between the specific volume and velocity profiles vanish. Since the energy equation is redundant, both the relative distance between the specific volume and energy profiles and relative energy do not exist.

3.3. Godunov method for isentropic equations

Godunov method does not define explicit viscosity. It solves Riemann problem at cell interface at first and then makes cell average. We will see below that the dissipative mechanism is similar to that of artificial method, but more complex.

Consider a general system of conservative laws

$$\frac{\partial U}{\partial t} + \frac{\partial F}{\partial \xi} = 0. \tag{20}$$

The Godunov method is

$$U_j^{n+1} = U_j^n - \frac{\Delta t}{\Delta \xi}\left(F_{j+1/2} - F_{j-1/2}\right), \tag{21}$$

where Δt and $\Delta\xi$ are temporal and spatial steplength. The numerical flux for most shock-capturing methods can be written as

$$F_{j+1/2} = \frac{1}{2}\left(F_j + F_{j+1}\right) - Q_{j+1/2}\Delta U_{j+1/2}, \tag{22}$$

where $\Delta U_{j+1/2} = U_{j+1} - U_j$, and $Q_{j+1/2}$ is a general numerical viscosity matrix.

Applying (22) to (21) one gets viscous modified equation

$$\frac{\partial U}{\partial t} + \frac{\partial F}{\partial \xi} = \frac{\partial}{\partial \xi}\left(\Delta\xi Q \frac{\partial U}{\partial \xi}\right).$$

For isentropic Eq. (4), $U = (\tau, u)^T,\ F = (-u, P)^T$. Using different Riemann solvers will result in different modified equations. For example, by using primitive variable Riemann solver [21], the fluxes are

$$\begin{aligned} u_{j+\frac{1}{2}} &= \frac{1}{2}(u_j + u_{j+1}) + \frac{1}{2}(P_j - P_{j+1})/\overline{\rho c}, \\ P_{j+\frac{1}{2}} &= \frac{1}{2}(P_j + P_{j+1}) + \frac{1}{2}(u_j - u_{j+1})\overline{\rho c}, \end{aligned} \tag{23}$$

where $\overline{\rho} = 0.5(\rho_j + \rho_{j+1}),\ \overline{c} = 0.5(c_j + c_{j+1})$. Substituting these fluxes into (21) and making Taylor expansion, we can obtain a first order modified Lagrangian system according to this kind of Godunov scheme

$$\begin{cases} \tau_t - u_\xi = -(\varepsilon_1 P_\xi)_\xi, \\ u_t + P_\xi = (\varepsilon_2 u_\xi)_\xi, \end{cases} \tag{24}$$

where $\varepsilon_1 = \Delta\xi/(\rho c),\ \varepsilon_2 = \Delta\xi\rho c$ are variable viscous coefficients.

Remark 2. Although the Godunov schemes have different forms for isentropic equations, such as using exact Riemann solver, Roe approximate solver [22] and HLL solver [23] etc., they all belong to a two-wave configuration for a hyperbolic system of two equations. So the first order modified equations have unique form (24). The discrepancies of different modified equations appear in higher order expansion terms.

Consider a right facing traveling shock wave solution at speed s with limiting state (τ_a, u_a) and (τ_b, u_b), [see (17)], then by Rankine–Hugoniot jump conditions there are

$$\begin{cases} u - \varepsilon_1 P_\xi = u_a - s(\tau - \tau_a) = u_b - s(\tau - \tau_b), \\ P - \varepsilon_2 u_\xi = P_a + s(u - u_a) = P_b + s(u - u_b). \end{cases}$$

Similarly define the shock positions of viscous profiles of specific volume and velocity by (19). Substituting the formulae

$$u - u_a = \varepsilon_1 P_\xi - s(\tau - \tau_a), u - u_b = \varepsilon_1 P_\xi - s(\tau - \tau_b)$$

into (19), we can obtain the relative distance between the front of velocity and specific volume profiles as

$$\delta_{u\tau} = \xi_s^u - \xi_s^\tau = \frac{\int_{-\infty}^{\infty} \varepsilon_1 P_\xi d\xi}{s(\tau_b - \tau_a)} < 0.$$

The relative momentum between the two fronts is

$$\delta M = \delta_{u\tau}(u_a - u_b) = \int_{-\infty}^{\infty} \varepsilon_1 P_\xi d\xi.$$

3.4. The Godunov method for adiabatic equations

From the viewpoint of modified equations, the Riemann solvers in Godunov method for adiabatic equations can be classified into two distinct categories. One is the three-wave solvers which can exactly resolve contact discontinuities, such as exact Riemann or HLLC solvers etc. [23]. Another is to assume a wave configuration for the solution which consists of two waves separating three constant states, which includes Lax–Friedrichs or HLL solver, etc. [23].

If we choose an approximate Riemann solver as (23), and the flux $F = (-u, P, uP)^T$ is obtained by this Riemann solver, then the first order modified equations for adiabatic models (2) are

$$\begin{cases} \tau_t - u_\xi = -(\varepsilon_1 P_\xi)_\xi, \\ u_t + P_\xi = (\varepsilon_2 u_\xi)_\xi, \\ E_t + (Pu)_\xi = (\varepsilon_1 PP_\xi)_\xi + (\varepsilon_2 uu_\xi)_\xi. \end{cases} \tag{25}$$

where $\varepsilon_1 = \Delta\xi/(\rho c),\ \varepsilon_2 = \Delta\xi\rho c$.

Suppose that a right facing shock wave at constant speed s exists, and its left and right limiting states are (8), then in the shock profile there are

$$\begin{cases} u - \varepsilon_1 P_\xi = u_a - s(\tau - \tau_a) = u_b - s(\tau - \tau_b), \\ P - \varepsilon_2 u_\xi = P_a + s(u - u_a) = P_b + s(u - u_b), \\ Pu - \varepsilon_1 PP_\xi - \varepsilon_2 uu_\xi = P_a u_a + s(E - E_a) = P_b u_b + s(E - E_b). \end{cases} \tag{26}$$

Define the shock positions of viscous profiles of specific volume, velocity and energy by (12). By similar analysis in Section 3.3, we know that the relative distance between the front of velocity and specific volume profile is $\delta_{u\tau} = \int_{-\infty}^{\infty} \varepsilon_1 P_\xi d\xi / s(\tau_b - \tau_a)$, and the relative momentum is $\delta M = \int_{-\infty}^{\infty} \varepsilon_1 P_\xi d\xi$.

The analysis of relative energy is difficult. By now there has not been any known expression of a traveling solution for this system of viscous equations like (10), so the shock position of energy profile cannot be determined exactly. In general, the shock position of energy profile does not coincide with that of specific volume profile. For example, when $\varepsilon_1 = 0$, the system is degenerated into artificial viscous equations, in which relative energy is nonvanishing.

The approximate Riemann solution (23) corresponds to a HLLC scheme with the signal velocities $\pm\overline{\rho c}$. If we adopt a HLL scheme with the same signal velocities, the numerical flux is

$$\begin{aligned} -u_{j+\frac{1}{2}} &= -\frac{1}{2}(u_j + u_{j+1}) - \frac{1}{2}\overline{\rho c}(\tau_{j+1} - \tau_j), \\ P_{j+\frac{1}{2}} &= \frac{1}{2}(P_j + P_{j+1}) - \frac{1}{2}\overline{\rho c}(u_{j+1} - u_j), \\ (Pu)_{j+\frac{1}{2}} &= \frac{1}{2}\left((Pu)_j + (Pu)_{j+1}\right) - \frac{1}{2}\overline{\rho c}(E_{j+1} - E_j). \end{aligned} \tag{27}$$

From the flux form, the modified equations of the HLL scheme can be obtained as

$$\begin{cases} \tau_t - u_\xi = -(\varepsilon\tau_\xi)_\xi, \\ u_t + P_\xi = (\varepsilon u_\xi)_\xi, \\ E_t + (Pu)_\xi = (\varepsilon E_\xi)_\xi, \end{cases} \tag{28}$$

where $\varepsilon = \Delta\xi\rho c$. If a right facing shock wave with constant speed s exists, then in the shock profile there are

$$\begin{cases} u + \varepsilon\tau_\xi = u_a - s(\tau - \tau_a) = u_b - s(\tau - \tau_b), \\ P - \varepsilon u_\xi = P_a + s(u - u_a) = P_b + s(u - u_b), \\ Pu - \varepsilon E_\xi = P_a u_a + s(E - E_a) = P_b u_b + s(E - E_b). \end{cases} \tag{29}$$

Similar to the previous analysis, we know that the relative distance between the velocity and specific volume profiles is $\delta_{u\tau} = -\int_{-\infty}^{\infty} \varepsilon\tau_\xi d\xi / s(\tau_b - \tau_a)$, and the relative momentum is $\delta M = -\int_{-\infty}^{\infty} \varepsilon\tau_\xi d\xi$. In general, the relative distance between energy profile and specific volume profile is nonvanishing, thus the relative energy no longer vanishes.

4. Behavior of viscous solution

If initial data corresponds to the viscous profile (10), the shock structure of (3) is the steady traveling wave (10). But for the jump type initial data, the solution does not correspond to the profiles in the viscous steady shock, therefore some reconstructions of the profiles begin, as a result, the solution asymptotically reaches the regime of shock structure.

4.1. Generation of entropy errors

The basic assumption is from [11]: when the fluid equations are regularized by a viscous dissipation term, a shock wave approaches its asymptotic traveling wave profile very rapidly. In fact this is a necessary condition for shock capturing algorithms in numerical method.

Such traveling shock profiles accumulate different energy from hyperbolic solution. The distribution manner of the extra energy depends on the dissipative mechanism of viscous equations. We will describe formation and propagation process of a viscous shock wave for von Neumann artificial Eq. (6) when exact discontinuity is used in initial data.

The evolution of viscous shock can be regarded as singular perturbation problem, the total time process can be decomposed into a fast and slow time scale [24,11]. On each scale the wave structure is the competing result of dissipative effect and hyperbolic property simultaneously.

Over the fast time scale, (effective shock width)/(shock velocity), the initial discontinuity U_0 is smoothed. On the one hand, viscosity results in the solution going to a stable traveling shock wave structure U. The fronts of the specific volume and energy U separate gradually from each other, and the relative distance and relative energy between these two fronts quickly change from 0 to $\delta_{E\tau}$ and from 0 to δE. On the other hand, according to Remark 1, the energy of viscous shock U is less than that of U_0. To satisfy energy conservation law, a perturbation U_1 is sure to be generated. U_1 propagates along the nonlinear acoustic wave and entropy wave, and diffuses to whole solution simultaneously. In addition, U_1 satisfies the following relations

$$\begin{aligned} &V_T(U_1) = V_T(U_0 - U) = 0, \\ &M_T(U_1) = M_T(U_0 - U) = 0, \\ &E_T(U_1) = E_T(U_0 - U) > 0. \end{aligned}$$

Under the interaction of dissipative mechanism ($u_{\xi\xi}$), the particle velocity in U_1 will be smoothed out rapidly and go to constant velocity state, but the particle velocity in U still preserves large gradient profile. Along with particle velocity of solution U_1 approaching to a constant, the pressure equilibrates to its values behind the shock almost at the same time. In the viscous adiabatic problem (6), due to lack of dissipation in energy, the energy in U_1 does not tend to be constant with the same rate of pressure equilibrium. Once velocity and pressure approach to constants, the energy and density will preserve their configuration almost invariably. There is a rise in energy near the contact wave. According to the equation of state $P = (\gamma - 1)\rho e$, a dip in density occurs.

On the slow time scale, the wave structure of viscous solution approaches the traveling shock wave asymptotically, and the relative distance between specific volume and energy fronts is close to a constant. New perturbation U_1 becomes so small that it can be negligible compared with those made on the fast time scale.

In summary, due to pressure and particle velocity approaching equilibrium, the perturbation U_1 forms its shape mainly on the fast time scale. The contribution on the slow time scale exists but small. A nonlinear acoustic wave error occurs near 1-wave, an overheating error flows with fluid particle as 2- wave (hereafter we also call it entropy error or overheating error), and the stable traveling shock is 3-wave. This discontinuity decomposition in viscous equations with small ε is similar to a general Riemann problem decomposition, which results in the generation of a whole fan of waves, and not just a 3-wave as expected from the initial data. When viscous coefficient is constant in Eq. (6), the relative energy does not result in postshock oscillations.

Remark 3. In viscous adiabatic Eq. (6), the overheating error locates near contact discontinuity and distributes in a region of $\delta(\varepsilon)$, where $\delta(\varepsilon)$ depends on the initial layer time and viscosity. There is not any knowledge about its distribution form. We will assume that the entropy error has a "smoothed" squared wave distribution if it is not dissipated by acoustic wave, then the peak value of such error is about

$$E_{\max}(U_1) \approx C \quad \delta E/\delta(\varepsilon). \tag{30}$$

In numerical computation, the steady overheating error always distributes in a few grids. According to the above assumption, if the error is not dissipated by acoustic wave, then the peak value is about

$$E_{\max}(U_1) \approx C \quad \delta E/\Delta\xi, \tag{31}$$

where C is a constant and $\Delta\xi$ is mesh spacing in the mass coordinate. The relation (31) will be verified by some numerical experiments in Section 4.2.

4.2. Numerical evidences

The relative energy formula and viscous shock structure in Section 4.1 can be checked by the numerical experiments. To avoid overheating error dissipated by propagation of 1-wave, we consider Noh problem [10] which is equivalent to a Riemann problem with an initial constant velocity directed towards each,

$$U_L = (\rho, u, P, E)_L = (1, 1, 0, 0.5), \quad \text{if } x < 0.5;$$
$$U_R = (\rho, u, P, E)_R = (1, -1, 0, 0.5), \quad \text{if } x > 0.5,$$

where specific heat ratio is 5/3. The 1-wave and 3-wave are shock waves, so relative energy concentrates on 2-wave. The exact solution consists of two symmetric shocks whose velocities are 4/3 and $-4/3$, respectively. The density and total energy of the postshock are 4 and 0.5, respectively.

Case 4.1. We use the same grid (400 zones) but different linear viscosity coefficients

$$\Delta t = 10^{-4}, \quad \varepsilon = k\Delta\xi.$$

The numerical energies at $k = 2.5,\ 3.0,\ 3.5$ are given in Fig. 2. Since the initial density is 1, the physical spacing $\Delta x = \rho\Delta\xi = \Delta\xi$. According to (15), the relative energy is a linear function of viscosity coefficient ε. By Remark 3, the peak values of overheating errors are almost in proportion to the factor k in viscosity coefficient. Fig. 3 gives some peak values of energies with respect to different k. The results coincide with (31) well. Note that such linear relation holds only under the circumstance of these viscous coefficients being on a certain range.

Case 4.2. Using a fixed viscosity coefficient factor $\varepsilon = 1.2\Delta\xi$ but with different grids $\Delta\xi$, the results are given in Fig. 4. The three cases are

$$\Delta t_1 = 10^{-3}, \quad \Delta\xi_1 = 0.01; \quad \Delta t_2 = 5.0 \times 10^{-4}, \quad \Delta\xi_2 = 0.005; \quad \Delta t_3 = 2.5 \times 10^{-4}, \quad \Delta\xi_3 = 0.0025.$$

The magnitude of overheating errors is almost the same, but the overheating error in spatial range decreases with grid refined. Similar numerical experiments lead Noh [10] to conclude that the error is built into the exact solution of viscous equations.

Remark 4. From the analysis in Section 4.1 and above numerical experiments, for any fixed ε the viscous shock solution with discontinuous initial data will not converge to a single viscous shock in L^1 as time goes to infinity. In addition, when $\Delta t/\Delta\xi = constant$ and $\Delta\xi \to 0$, the numerical solution will converge to an inviscid limit. The Case 4.2 shows that the viscous shock solution with constant peak value entropy error will not converge to a discontinuous shock solution in L^∞ as $\varepsilon \to 0$ (see [11,10]).

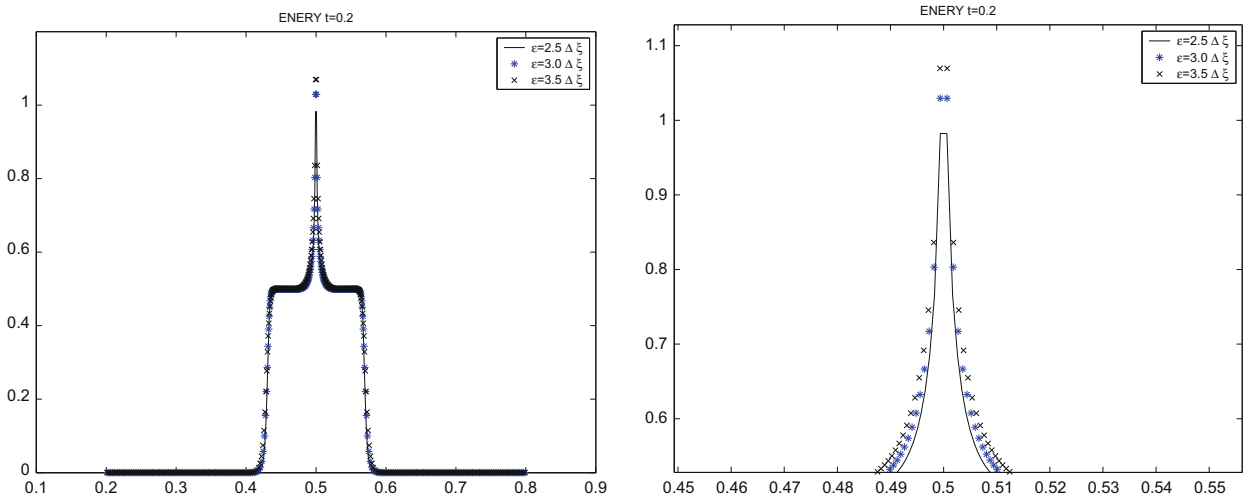

Fig. 2. Energy errors with different viscosity coefficients but the same grid. Left: energy at $t = 0.2$, right: magnification of the same results.

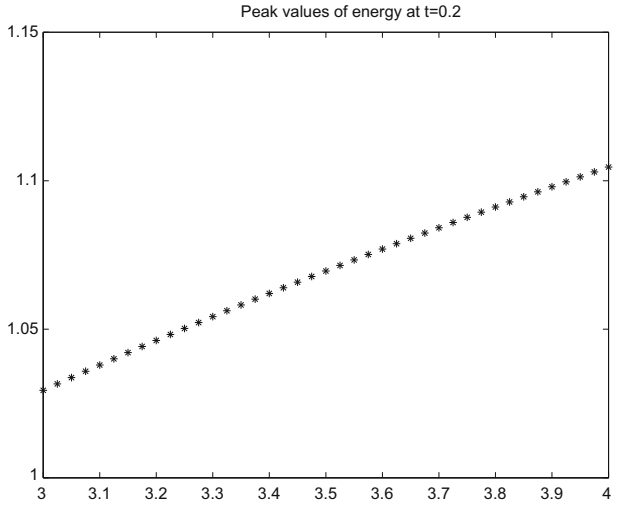

Fig. 3. Energy peak values with different viscosity coefficient relation k but the same grid. x-Coordinate is k.

Case 4.3. Consider the following shock reflection problems with initial conditions:

$$U_L = (\rho, u, P, E)_L = (4, 1, 4/3, 1), \quad \text{if } x < 0.2;$$
$$U_M = (\rho, u, P, E)_M = (1, 0, 0, 0), \quad \text{if } 0.2 < x < 0.8;$$
$$U_R = (\rho, u, P, E)_R = (4, -1, 4/3, 1), \quad \text{if } x > 0.8,$$

where specific heat ratio is 5/3. The head-on collision problem of two equal strength shock waves is equivalent to shock reflecting from a rigid wall exactly for inviscid hydrodynamic equations. That means it is equivalent to the following Riemann problem:

$$U_L = (\rho, u, P, E)_L = (4, 1, 4/3, 1), \quad \text{if } x < 0.5;$$
$$U_R = (\rho, u, P, E)_R = (4, -1, 4/3, 1), \quad \text{if } x > 0.5.$$

The reflective shock has the state:

$$U = (\rho, u, P, E) = (10, 0, 8, 1.2).$$

But viscous shock behavior would be different for these processes. In fact, it includes two physical processes(see Fig. 5). When the viscous incident shock interacts on the rigid wall (state (0) to state (1)), the relative distance decreases, and the absolute value of relative energy increases, which is $\delta E_i = \frac{2}{(\gamma+1)}\varepsilon c_0$. The viscous shock wave contains more energy than that with constant relative distance, so the overcooling phenomenon will appear. When the reflected shock leaves the rigid wall (state (1) to state (2)), the relative distance increases and the solution approaches to constant velocity traveling wave, and

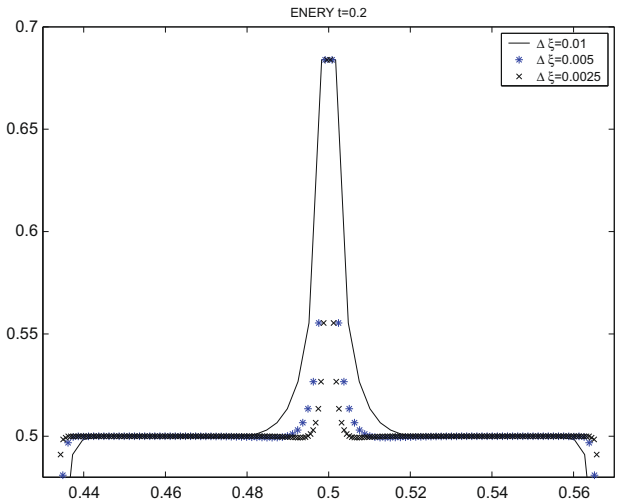

Fig. 4. Energy errors with different grids but fixed viscosity relation $\varepsilon = 1.2\Delta\xi$.

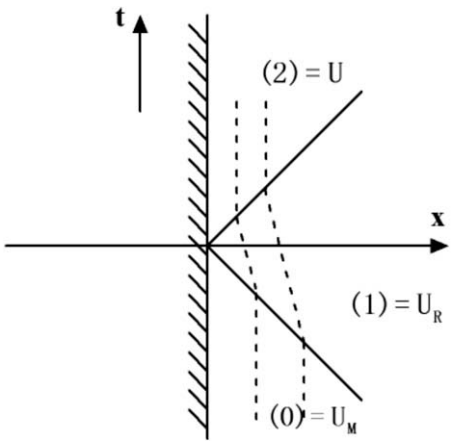

Fig. 5. Reflection of a shock wave on a rigid wall.

the released relative energy in traveling wave solution is $\delta E_R = -\frac{2}{(\gamma+1)}\varepsilon c_0$. In principle the two effects should exactly cancel out, but numerically they typically illustrate the wall heating phenomenon. The reason is as follows: the partially added energy in incident shock profile is deficit by its acoustic wave propagation to postshock, but the reduced relative energy in reflected shock almost preserves all entropy error near the rigid wall, so the total effect exhibits the wall heating phenomenon. Fig. 6 gives energy and density solutions, in which the overheating errors are obvious. But this conclusion is not true to other viscous equations and other numerical methods. We will see the different results in Section 4.3.

4.3. Extension to other viscous equations

The shock generation process for artificial viscosity Eq. (6) also can be extended to other viscous equations.

For viscous isentropic Eq. (16), there is no relative distance, relative momentum and energy. That means there is no difference between viscous solution and hyperbolic solution in integral meaning. What will happen when jump type initial values are used? Whether there exists a single viscous shock family? Hoff and Liu provided a picture to qualitative properties of this solution [24]: in a very short time, the initial discontinuity decays exponentially in time. For intermediate time the solution is approximated well by solutions of Burgers equation, appropriately lifted to phase space. For large time, the solution coincides with the viscous traveling wave solution very well. From the picture we can conclude that the viscous solution keeps the monotony and convergence to a single viscous shock as time goes to infinity. But in our numerical experiments using artificial viscosity method, a perturbation U_1 can be always observed near 1-wave, and is dissipated soon in time. How to explain such perturbation generation is still an open problem. We call such error as high order one in integral mean-

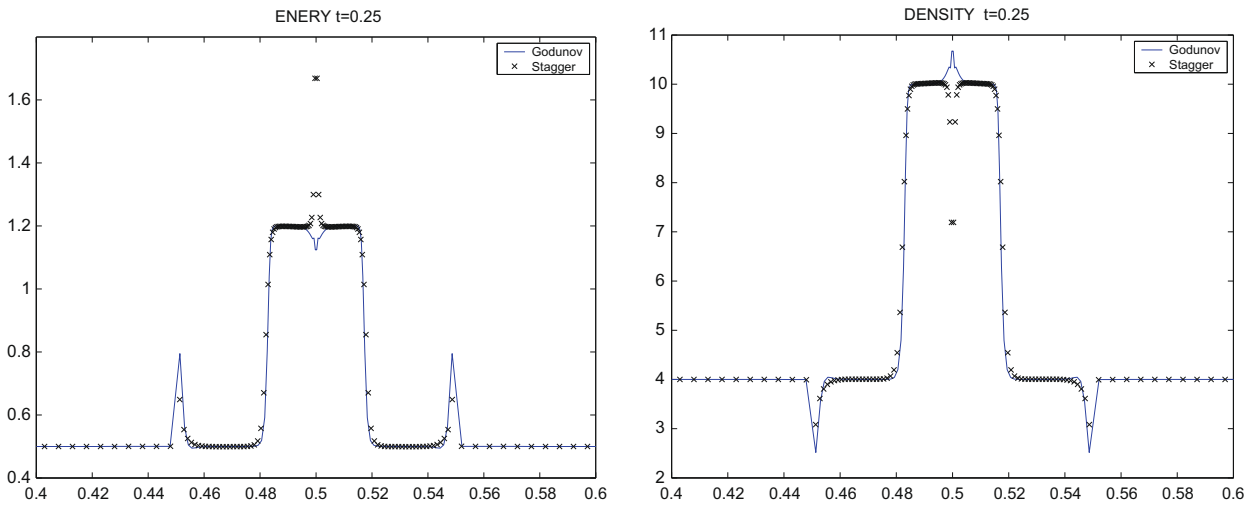

Fig. 6. Interaction of viscous shock. The cross is the von Neumann method, and the line is Godunov method. Left: specific internal energy, right: density.

ing compared with overheating error as first order error. In viscous adiabatic Eq. (6), the perturbation U_1 includes such high order error (start up error).

For viscous isentropic Eq. (24), the relative momentum exists. During the fast time scale, 1-wave error is generated. Under the interaction of dissipative mechanism ($u_{\xi\xi}$), the 1-wave error will be smoothed out rapidly. Due to the relative momentum vanishing in (16) but not so in (24), the strength of perturbation U_1 is different. This will be exhibited in the postshock oscillation numerical experiments in Section 5.2.

Remark 5. For any fixed ε, the viscous shock solution in (24) with discontinuous initial data will not converge to a single viscous shock in L^1 as time goes to infinity.

For viscous adiabatic Eq. (25) obtained from Godunov scheme, the dissipative mechanism is similar to (6), but the situation is more complex. The viscous solution includes relative momentum and relative energy. During the fast time process, a perturbation U_1 is generated and decomposed into acoustic wave errors and an entropy wave error. Under the interaction of dissipative mechanism $u_{\xi\xi}$ and $P_{\xi\xi}$, the particle velocity and pressure in U_1 will approach to constants rapidly, but the particle velocity and pressure in U still preserve large gradient profile. Due to lack of dissipation in energy, the energy in U_1 will preserve their configuration almost invariably. If relative energy is negative, there will be a wall heating error near the contact wave, otherwise a wall cooling phenomenon will appear. In the viscous equations, viscous term $P_{\xi\xi}$ will help to attain pressure and velocity equilibrium more quickly than that from von Neumann artificial viscosity method will do.

In numerical Godunov method, the dissipation is implicit, and viscous coefficient is no longer constant. The uncontrollable and adaptive viscosity in (25) may become a latent harmful factor, but also may lessen extent of error. Let us use a shock interaction example in Section 4.2 to illustrate its complexity.

Fig. 6 compares the difference between Godunov method and von Neumann method when viscous shock interaction is computed. The artificial viscosity method always exhibits overheating phenomenon, while Godunov method has an overcooling error. It shows that the relative energy during the incident process from state (0) to (1) (see Fig. 5) is larger than that during the reflective process, i.e., $|\delta E_i| > |\delta E_R|$.

5. Effect of variable viscosity

So far we have just discussed the case in which viscosity ε is constant. Now we want to know what will happen when ε varies. Without loss of generality, we just discuss Eq. (6) with artificial viscosity (7). Suppose that there is a stable viscous shock propagation at constant speed s, we denote its relative energy by δE_{old} . If ε changes, for example increases, then transition zone of viscous shock will increase, so perturbation U_1 is generated. The viscous effect decays the perturbation into whole domain. Whether there is visible oscillatory phenomenon depends on the balance between oscillation amplitude and dissipation velocity. For the adiabatic problem the relative distance between different fronts increases, and the relative energy in new traveling shock satisfies $\delta E_{new} < \delta E_{old}$. The energy in previous stable profile will release and give rise to "wall heating" phenomenon. If wave strength is large enough or ε changes acutely, then the dissipation term in von Neumann method usually cannot prevent postshock oscillations. Conversely when ε decreases, the solution will experience overcooling effect, i.e., a rise in density and a dip in energy. Similar analysis can be extended to the other viscosity equations. Two examples are exhibited below.

5.1. Nonuniform grid

During numerical calculation mesh variation will produce such effect: as a shock passes through a mesh spacing changing from a finer to a coarser or reverse, the viscous coefficient as a function of mesh spacing will change.

Consider a planar shock crossing the boundary between a coarser to a finer mesh and back from a finer to a coarser mesh [25]. A computational solution for classical Noh problem is shown for two 2:1 mesh variations in Fig. 7(a). The problem is set up as follows:

Case 5.1

$$\begin{cases} x \in (0, 20/65] \cup (45/65, 1], & \Delta x = 1/65; \\ x \in (20/65, 30/65] \cup (35/65, 45/65], & \Delta x = 1/130; \\ x \in (30/65, 35/65], & \Delta x = 1/200, \end{cases}$$

where a piston with velocity 1 pushes a rest gas with state $U = (\rho, u, P) = (1, 0, 10^{-6})$. Notice here initial spatial steplength is $\Delta x = \Delta\xi$, and the viscosity coefficient is selected as $\varepsilon = 1.5\Delta\xi,\ c_0 = 1$.

The overheating phenomenon occurs precisely where the mesh increases its spacing and grows worse as the size of the mesh variation grows. Conversely, the solution experiences overcooling where the mesh is refined. In this figure perturbation which propagates through acoustic wave (1-wave) is not obvious due to dissipative.

For the viscous isentropic equations, the sudden change of viscosity ε causes new wave family generated. Fig. 7(b) gives the result of following example.

Case 5.2. A piston with velocity 1 pushes a rest gas with state $U = (\rho, u) = (1, 0)$, where pressure $P = \rho^{\gamma},\ \gamma = 5/3$. The other conditions are the same as Case 5.1, such as grid, spatial and temporal steplength and viscosity coefficient.

The exact solution is still a single shock. Since there does not exist relative distance, downstream oscillation is generated but amplitude is small.

5.2. Postshock oscillations

From mathematical analysis in Section 4.1, it is shown that there is no oscillations generated in constant ε viscous equations. However almost all shock capturing schemes for the moving shocks give postshock oscillations. Xu and Hu ascribe it to the unsteadiness of dissipative mechanism [8]. We agree on their argument completely and complement more details in Lagrangian framework. For the Godunov method, the viscosity term is introduced by cell average, which is implicit and adaptive to physical quantities (density and sound speed). When shock moves in a mesh during many time steps (slowly moving shock case), the cell average results in the viscosity variation. Therefore postshock oscillation is generated. The relative momentum and energy enlarge the oscillation amplitude. For the artificial viscosity method, how to explain postshock oscillation is difficult in the case of constant viscosity coefficient and uniform grid. In fact in slowly moving shock case the entropy error generating zone and viscous shock transition zone stick all the time. The velocity gradient obtained by finite difference in the vicinity of shock cell always gives rise to changes of viscous coefficients. It is such unsteadiness that results in postshock oscillation.

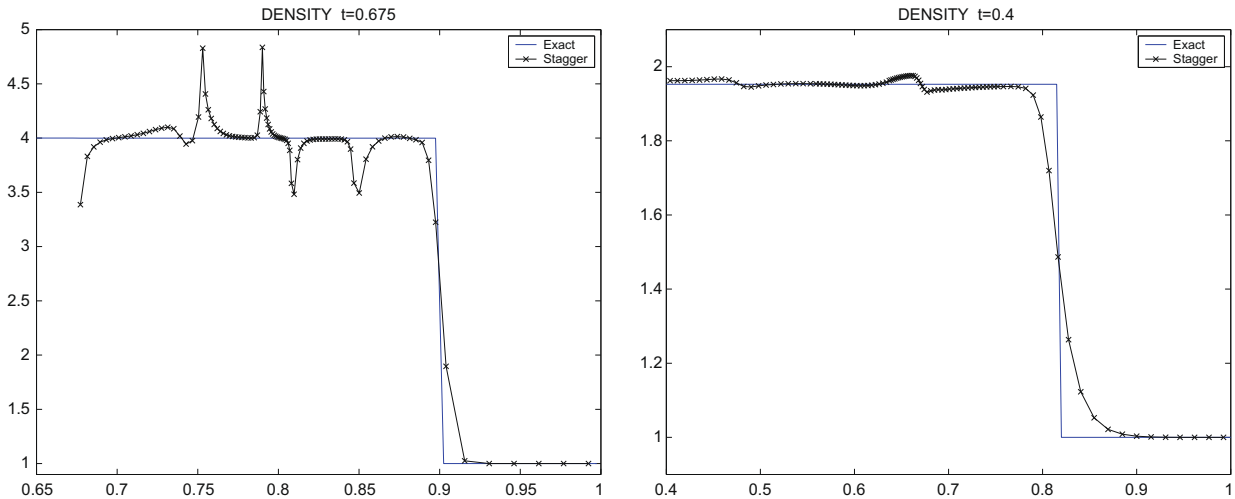

Fig. 7. Numerical solution with nonuniform grid. (a) Adiabatic problem (Noh), (b) isentropic problem.

A worthwhile discussion is isentropic equations with constant viscosity coefficient. Both its relative energy and relative momentum vanish in this case. In principle the postshock oscillations should not exist when using the artificial viscosity method and uniform grid. Since the numerical velocity gradient may vary near shock cell, there are some perturbations generated along with viscosity variety. But the extent of the oscillations is so small compared with Godunov method that the oscillations are almost invisible in some cases.

Case 5.3. Consider a Riemann problem

$$U_L = (\rho, u)_L = (1, 10), \quad \text{if } x < 0.5;$$
$$U_R = (\rho, u)_R = (1, -10), \quad \text{if } x > 0.5,$$

where $P = \rho^2$. In this example, the same grid (200 zones) is used and the viscosity coefficient is $\varepsilon = 10\Delta\xi,\ c_0 = 1$. The postshock density is 10.5576.

Fig. 8 compares the results of a shock collision problem for isentropic equations computed by two different methods. The numerical results show that Godunov method has strong oscillations, while artificial viscosity method has almost free oscillations. Of course, if increasing shock strength such as $U_L = (1, 100),\ U_R = (1, -100)$ and keeping the viscosity be invariable, the postshock oscillation in the artificial viscosity will still be generated. If we increase viscosity correspondingly, for example, $\varepsilon = 50\Delta\xi$, the postshock oscillations vanish once more.

6. Extend to rarefaction waves

From the energy argument based on the shock profiles, we conjecture that the same behavior occurs for a viscous rarefaction wave. For the jump type initial data satisfying single rarefaction wave condition, the solution includes not only stable viscous solution but an entropy error and other perturbation. Although lacking of analytic solution like (10) to provide explicit relative energy and relative momentum, we still use an example to illustrate the entropy error.

Case 6.1. Consider a Riemann (123) problem with initial data

$$U_L = (\rho, u, P, E)_L = (1, -2, 0.4, 3), \quad \text{if } x < 0.5;$$
$$U_R = (\rho, u, P, E)_R = (1, 2, 0.4, 3), \quad \text{if } x > 0.5,$$

where the specific heat ratio is 1.4.

The exact solution consists of two symmetric rarefaction waves and a trivial contact wave of zero speed; the contact discontinuity region between the nonlinear waves is close to vacuum, which makes this problem a suitable test for assessing the performance of numerical methods for low density flows [26]. The performance of Godunov's method is generally quite satisfactory as regards the physical variables u and P, but not so much for the specific internal energy, see Fig. 9(b). People usually regard that both pressure and density are close to zero and thus small errors will be exaggerated by their ratio. Here we ascribe it to too much overheating error. Fig. 9 compares some solutions of artificial viscosity and Godunov method with different spatial steplength. The viscosity in artificial viscosity method is implemented constrainedly whether it treats shock or rarefaction wave. They exhibit the similar form and show that the error source is the same. In classical artificial viscosity

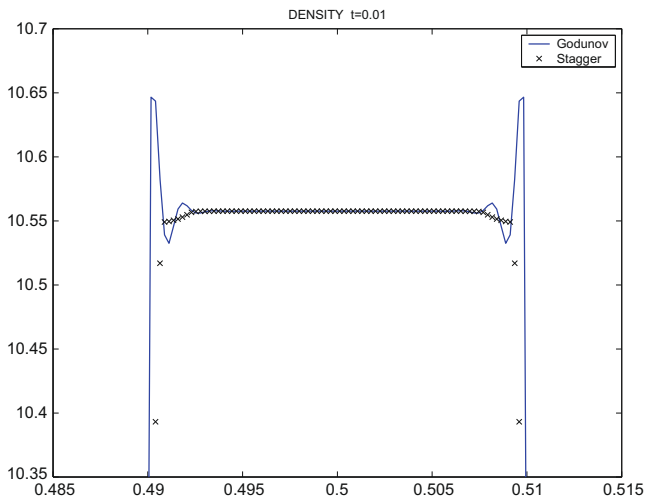

Fig. 8. Postshock oscillation of Godunov method and artificial viscous method.

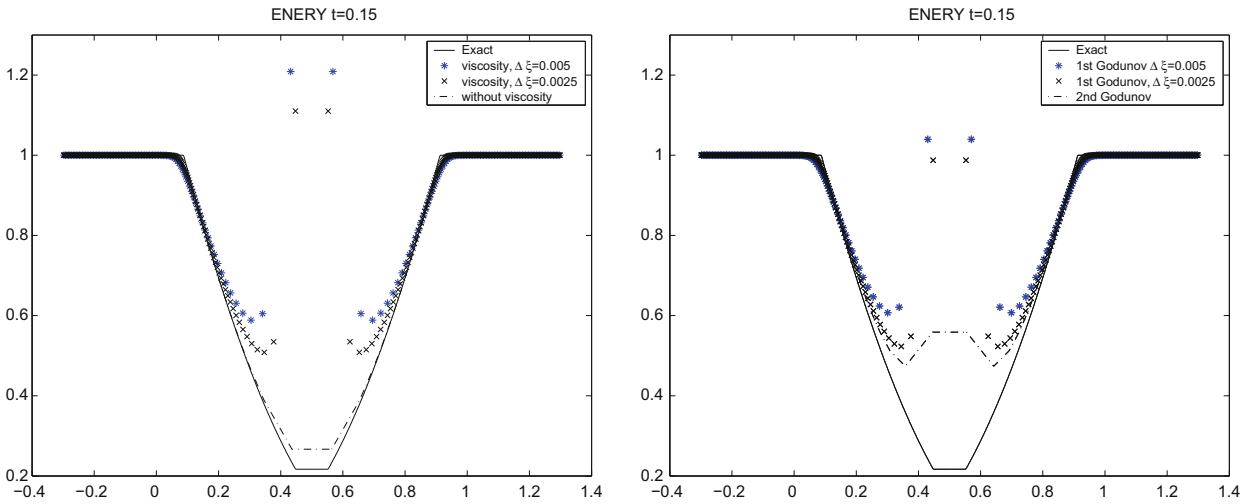

Fig. 9. Numerical solutions to 123 problem with different grids. (a) Artificial viscosity method, (b) Godunov method.

method viscosity is usually taken to zero in region of rarefaction wave, so entropy errors do not appear. The dot line in Fig. 9(a) is the result without viscosity. For Godunov method, cell average of flow variables introduces viscosity naturally, so entropy error is inevitable (Fig. 9(b)).

7. The methods to ameliorate or eliminate entropy error

Since the entropy error and momentum error are caused by the viscosity in the numerical scheme, reducing the viscosity as much as possible or diffusing perturbation will ameliorate even eliminate this type of error.

Two types of methods can completely eliminate viscous error. One is the Random Choice Method (RCM) introduced by Glimm [27] and developed by Chorin and co-workers [28–31], another is shock tracking method [32,14]. Both of them adopt exact solutions of local Riemann problems. After solving a Riemann problem at the interface of two cells, RCM uses a random sampling procedure to pick up states instead of averaging the resulting solutions over grid cell to assign to the next time level. The basic idea of shock tracking method is splitting a computational cell containing a shock wave along the trajectory of the shock. The split shock cell becomes two subcells: one is entirely upstream of the shock and the other is entirely downstream. It avoids taking an integral average on a shock grid cell. The entropy errors are eliminated completely, and shock has infinite resolution in these two kinds of methods. But these methods confront similar embarrassment when problems with complex equation of state are solved. Moreover, the extension to multidimensional cases is very difficult in Lagrangian formulation.

7.1. High order scheme

In order to reduce the acoustic wave error and overheating error in fluid calculation, we require a high order interpolation in scheme to make the discontinuity between left state U_L and right state U_R as small as possible. For von Neumann viscosity method, the truncation errors on space and time have attained 2nd order accuracy, and implementing higher order scheme in a stagger grid is no longer easy. For Godunov method, there are a variety of reconstruction procedures available to increase the formal order of spatial and time accuracy of the method. In our experiments, we have chosen the high resolution scheme from wave propagation method [33].

Solving a system (20) including three-wave families gives the flux as

$$F_{j+1/2} = F\left(U^*_{j+1/2}\right) + \frac{1}{2}\sum_{p=1}^{3}\left|s^p_{j+1/2}\right|\left(1 - \frac{\Delta t}{\Delta\xi}\left|s^p_{j+1/2}\right|\right)\widetilde{W}^p_{j+1/2}, \tag{32}$$

where $U^*_{j+1/2}$ is the state on contact discontinuity from exact Riemann solver. $W^p_{j+1/2}$ is the pth wave arising in the solution to the Riemann problem at $\xi_{j+1/2}$, which propagates at the speed $s^p_{j+1/2}$. It satisfies

$$U_{j+1} - U_j = \sum_{p=1}^{3} W^p_{j+1/2},$$

and

$$F_{j+1} - F_j = \sum_{p=1}^{3} s_{j+1/2}^p W_{j+1/2}^p. \tag{33}$$

When the pth wave is shock wave (jump), $s_{j+1/2}^p$ is the shock velocity in Lagrangian coordinate. When the pth wave is contact wave, $s_{j+1/2}^p = 0$. However, rarefaction waves do not have a single wave speed $s_{j+1/2}^p$ to use in (32). Instead, the characteristic speed λ^p varies continuously through the rarefaction wave. Here we adopt an average speed, e.g. $s^p = 0.5(\lambda_l^p + \lambda_r^p)$. λ_l^p, λ_r^p are speed of rarefaction wave head and tail. The concrete formulation can be found in Appendix B. $\widetilde{W}_{j+1/2}^p$ is a limited version of wave $W_{j+1/2}^p$,

$$\widetilde{W}_{j+1/2}^p = \phi\left(\theta_{j+1/2}^p\right) W_{j+1/2}^p, \tag{34}$$

$\theta_{j+1/2}^p$ should be some measure of the smoothness of the pth characteristic component of the solution. It is easily obtained by comparing this jump with $W_{j+1/2}^p$ in the same family at the neighboring Riemann problem in the upwind direction. Denote

$$J = \begin{cases} j, & \text{if } s_{j+1/2}^p > 0, \\ j+1, & \text{if } s_{j+1/2}^p < 0, \end{cases} \tag{35}$$

then

$$\theta_{j+1/2}^p = \frac{W_{j+1/2}^p \cdot W_{j+1/2}^p}{W_{j+1/2}^p \cdot W_{j+1/2}^p}. \tag{36}$$

ϕ is a high resolution limiter, for example, $\phi(\theta) = minmod(1, \theta)$.

The use of high order scheme for a rarefaction wave and a single shock wave problems all can achieve certain effects. Figs. 9(b) and 10 include the second order results in rarefaction wave and shock wave, respectively. The overheating errors are significantly reduced in amplitude using the second order scheme. However, in high resolution TVD schemes, the reconstruction of numerical fluxes or conservation quantities need to meet TVD property. It is well known such scheme gives rather poor accuracy at extreme, even though the solution is smooth [34]. When the shock of collision reflection problem is computed, the slope of reconstructed function near the reflected wall is 0, and the method degenerates into first order accuracy, so overheating error is difficult to decline. ENO (essentially non-oscillatory) techniques [35,36] and PHM (piecewise hyperbolic method) [37] use a local adaptive stencil to obtain information automatically from regions of smoothness when the solution develops discontinuities. They give a reconstruction that allows smooth peaks to be better represented over time. We believe they should be able to obtain better results. However the ability to reduce entropy errors by high resolution methods is limited, they can lessen the amount of the entropy error than first order scheme, but cannot eliminate such errors.

7.2. Dissipative scheme

According to analysis in this paper, the entropy error and acoustic wave error in Godunov method for adiabatic equations seem inevitable. Redistributing these errors to whole solution is an effective way in obtaining reliable results. Among the

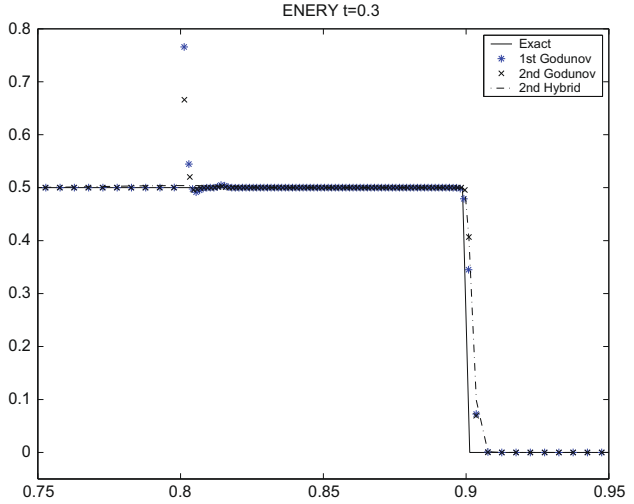

Fig. 10. Numerical solutions to Noh problem with different Godunov methods.

different shock-capturing methods, HLL or Local Lax Friedrichs (LLF) scheme [16] may be the most effective one to suppress overheating errors and postshock oscillations. In fact, these methods assume that a wave configuration for the solution consists of two-waves separating three constant states, and the HLL flux can be expressed by

$$F^{HLL}_{j+\frac{1}{2}} = \frac{s^3_{j+1/2}F_j - s^1_{j+1/2}F_{j+1} + s^1_{j+1/2}s^3_{j+1/2}(U_{j+1} - U_j)}{s^3_{j+1/2} - s^1_{j+1/2}},$$

where $s^p_{j+1/2}$ $(p = 1, 2, 3)$ is the wave velocity as described in Section 7.1, whose formulae can be found in Appendix B for the adiabatic model.

For this flux form, the modified equations of HLL scheme are the same as (28), in which the viscous terms include $\tau_{\xi\xi}$, $u_{\xi\xi}$ and $E_{\xi\xi}$. For an initial discontinuous shock data, the relative momentum and relative energy in viscous solution will result in a perturbation generated. On the one hand, in the interaction of these dissipative terms ($\tau_{\xi\xi}$, $u_{\xi\xi}$ and $E_{\xi\xi}$), the perturbation is smoothed out and the overheating errors are dissipated to whole solution. But on the other hand, the amount of viscosity in numerical scheme may be very large. The actual effect of these two factors depends on problems and cannot counteract in general, so entropy errors may still exist. Using high order HLL (LLF) scheme can modify the numerical results furthermore but the ability may be limited. Fig. 11 gives numerical solutions to 123 problem, and the strong entropy errors show that the viscosity in numerical solution is still too much. In addition, there exists other disadvantage using HLL scheme: the contact discontinuity cannot be captured sharply. When the fluids include different materials, how to distinguish sharp material interface is no longer easy and natural.

7.3. Hybrid scheme

It has a long history in computational hydrodynamics to combine a dissipative solver with a less dissipative one. Quirk [3] described a method to combine Roe scheme and other more dissipative solvers to control certain instabilities. Donat and Marquina [38] combined HLL scheme and other scheme to capture shock reflection and made very good results. The merit of such method is that it does not need to increase the absolute level of dissipation. The key point is when and where to use a Riemann solver in preference to another.

Here a simple hybrid scheme in Lagrangian coordinate is proposed. First we apply Godunov method in mass and momentum equations, and use HLL method in energy equation, then we will use high resolution scheme to implement calculation. The concrete scheme can be found in Appendix B. The basic idea is that since the entropy errors come from relative energy, and the dissipation should be set in energy equation. Of course, this hybrid method is not the best one to compute many problems. We can devise a more elaborate hybrid scheme to alleviate viscosity and obtain better results, such as using the HLL type Riemann solver locally in energy equation. But for the purpose of exhibiting a mechanism to suppress overheating phenomenon the simple method is enough. Figs. 10 and 11 illustrate the ability to calculate shock and rarefaction wave. In both cases, the entropy errors are suppressed very well.

For a general initial value problem, the hybrid scheme should show more numerical dissipation near contact discontinuity than classical Godunov and the artificial viscosity method, but higher resolution than HLL scheme. Here we consider two shock tube problems and compare the specific internal energies in different numerical schemes: the Godunov's second order method in conjunction with exact Riemann and HLL solvers, von Neumann viscosity method, and hybrid method.

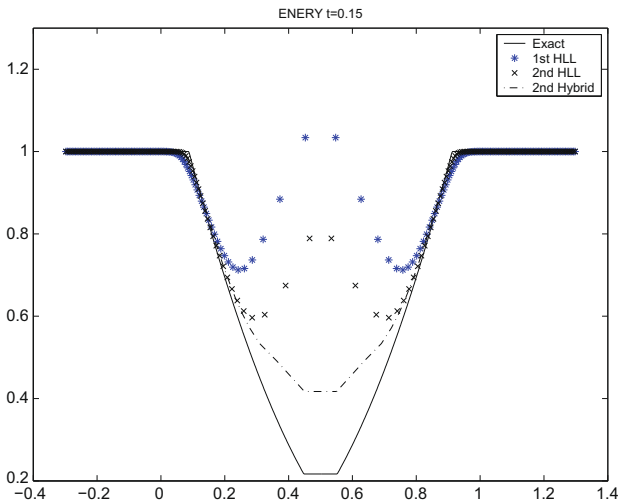

Fig. 11. Numerical solutions to 123 problem with different HLL methods.

Case 7.1. Consider a Riemann (Sod [39]) problem with initial data

$$U_L = (\rho, u, P)_L = (1, 0, 1.0), \quad \text{if } x < 0.4;$$
$$U_R = (\rho, u, P)_R = (0.125, 0, 0.1), \quad \text{if } x > 0.4.$$

Case 7.2. Consider a Riemann (shock collision [21]) problem with initial data

$$U_L = (\rho, u, P)_L = (5.99924, 19.5975, 460.894), \quad \text{if } x < 0.4;$$
$$U_R = (\rho, u, P)_R = (5.99242, -6.19633, 46.0950), \quad \text{if } x > 0.4,$$

where for each case the specific heat ratio is 1.4.

Fig. 12 gives some numerical results on Sod problem, in which computing domain is [0,1] and initial uniform physical grid cells (200 zones) are adopted as $\Delta x = 0.005$. The viscosity coefficient in each grid cell i for von Neumann method is $\varepsilon_i = 1.5\Delta\xi_i = 1.5\rho_i^0\Delta x$. The results show that the traditional Lagrangian methods have very good resolution on contact wave except overheating error. The hybrid scheme keeps high resolution for shock and cancels wall heating errors very well as predicted by the previous analysis. But it has a smeared contact wave like the HLL scheme although it is slightly better than the HLL one.

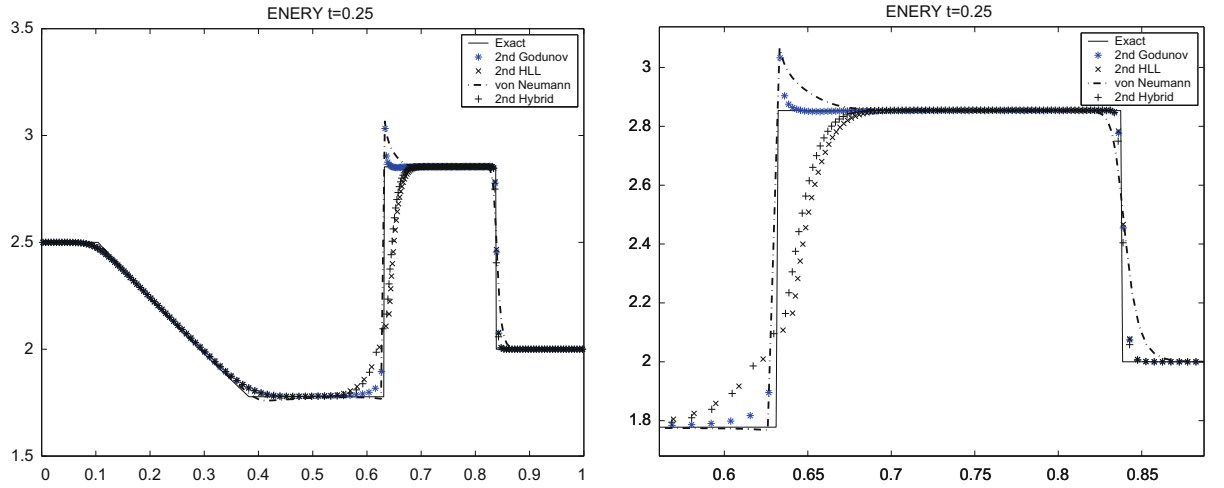

Fig. 12. Numerical comparisons to shock collision problem with different methods. Left: energy at $t = 0.25$, right: magnification.

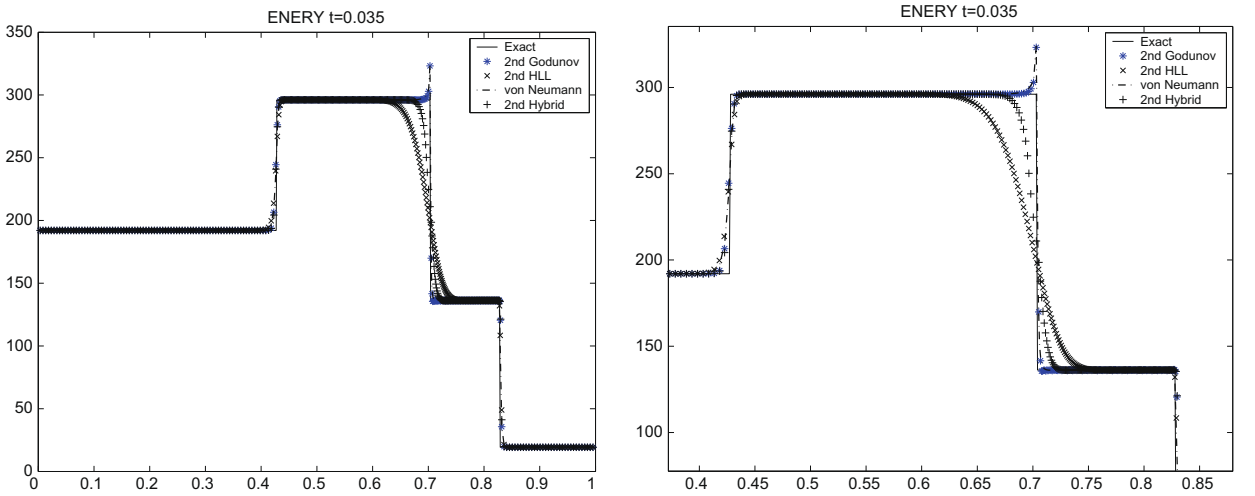

Fig. 13. Numerical comparisons to shock collision problem with different methods. Left: energy at $t = 0.035$, right: magnification.

The similar behavior is shown in Fig. 13 (Case 7.2). In this test, more grid cells (800 zones) are used due to its moving domain. The initial computing domain is $[-2,2]$ and the uniform physical grid spacing is $\Delta x = 0.005$. The viscosity coefficient in each grid cell i for von Neumann method is $\varepsilon_i = 8\Delta\xi_i$. The hybrid scheme diffuses the contact wave and overcomes the overheating error. In addition, it has an obvious advantage over the HLL scheme in this case.

8. Conclusions

We have analyzed the relation between viscous shock and inviscid one, and have described procedure of a viscous shock formation and propagation with a jump type initial data. In general, a viscous shock and an inviscid shock include different energy and momentum. The shifts between them are denoted by relative energy and relative momentum. These shifts will result in the generation of waves in all families when a single wave Riemann problem (shock or rarefaction) is solved. Being lack of suitable dissipation, entropy error will be generated. Employing this method, much anomalous behavior is explained well. Some reviews are given to those methods which can ameliorate even eliminate entropy errors. A concrete suggestion is that constructing scheme should consider both high resolution and dissipation in energy equation. Based on the understanding of behavior of viscous solution, a hybrid method is proposed and exhibits very good performance in suppressing wall heating errors. The next step is to develop an adaptive hybrid scheme in Lagrangian formulation to alleviate wall heating error and extend to the high dimensional problems.

Acknowledgments

This project was supported by the National Natural Science Foundation of China (10871029), the Foundation of CAEP (2008B0202021) and foundation of LCP, Basic Research Project of National Defence (A1520070074). The authors thank the reviewer's valuable suggestions during the revision of the paper.

Appendix A. The quadratic form viscosity

Consider Eq. (6) with quadratic form viscosity [1],

$$q = \begin{cases} \varepsilon^2\rho(\partial u/\partial\xi)^2, & \text{if } \partial u/\partial\xi < 0; \\ 0, & \text{others.} \end{cases} \tag{A1}$$

Denote $\xi_b = -\xi_a = \varepsilon\pi\sqrt{2/(\gamma+1)}/2$, then the steady shock transition zone is in $[\xi_a, \xi_b]$. The solutions of viscous Eq. (6) are

$$\begin{aligned} &(\tau, u, P, q, E) = (\tau_a, u_a, P_a, 0, E_a), \quad \xi < \xi_a + st; \\ &(\tau, u, P, q, E) = (\tau_b, u_b, P_b, 0, E_b), \quad \xi > \xi_b + st. \end{aligned} \tag{A2}$$

If $\xi_a < \xi - st < \xi_b$, the viscous profile of transition zone of (6) (see [40]) is

$$\begin{aligned} \tau &= \frac{\tau_b+\tau_a}{2} + \frac{\tau_b-\tau_a}{2}\sin\sqrt{\frac{\gamma+1}{2}}\frac{\xi-st}{\varepsilon}, \\ u &= \frac{u_b+u_a}{2} + \frac{u_b-u_a}{2}\sin\sqrt{\frac{\gamma+1}{2}}\frac{\xi-st}{\varepsilon}, \\ P+q &= \frac{P_b+P_a}{2} + \frac{P_b-P_a}{2}\sin\sqrt{\frac{\gamma+1}{2}}\frac{\xi-st}{\varepsilon}, \\ E &= \frac{E_b+E_a}{2} + \frac{E_b-E_a}{2}\sin\sqrt{\frac{\gamma+1}{2}}\frac{\xi-st}{\varepsilon} - \frac{(u_b-u_a)^2}{4}\cos^2\sqrt{\frac{\gamma+1}{2}}\frac{\xi-st}{\varepsilon}. \end{aligned} \tag{A3}$$

Define the shock positions of viscous profiles

$$\int_{\xi_a}^{\xi_s^\tau}(\tau-\tau_a)d\xi + \int_{\xi_s^\tau}^{\xi_b}(\tau-\tau_b)d\xi = 0, \quad \text{(i)}$$
$$\int_{\xi_a}^{\xi_s^u}(u-u_a)d\xi + \int_{\xi_s^u}^{\xi_b}(u-u_b)d\xi = 0, \quad \text{(ii)}$$
$$\int_{\xi_a}^{\xi_s^E}(E-E_a)d\xi + \int_{\xi_s^E}^{\xi_b}(E-E_b)d\xi = 0. \quad \text{(iii)}$$

After simple algebra, there are

$$\xi_s^\tau = (\tau_a - \tau_b)^{-1} \int_{\xi_a}^{\xi_b} (\tau - \tau_b) d\xi,$$

$$\xi_s^u = (u_a - u_b)^{-1} \int_{\xi_a}^{\xi_b} (u - u_b) d\xi,$$

$$\xi_s^E = (E_a - E_b)^{-1} \int_{\xi_a}^{\xi_b} (E - E_b) d\xi.$$

There are

$$\xi_s^\tau = 0, \quad \xi_s^u = 0, \quad \xi_s^E = -\frac{(u_b - u_a)^2}{4(E_b - E_a)} \pi\varepsilon \sqrt{\frac{1}{2(\gamma+1)}}.$$

The relative distance is

$$\delta_{E\tau} = \xi_s^E - \xi_s^\tau = -\frac{(u_b - u_a)^2}{4(E_b - E_a)} \pi\varepsilon \sqrt{\frac{1}{2(\gamma+1)}}. \tag{A4}$$

The relative momentum is

$$\delta M = \int_{\xi_a}^{\xi_s^\tau} (u - u_a) d\xi + \int_{\xi_s^\tau}^{\xi_b} (u - u_b) d\xi = 0. \tag{A5}$$

The relative energy is

$$\delta E = \int_{\xi_a}^{\xi_s^\tau} (E - E_a) d\xi + \int_{\xi_s^\tau}^{\xi_b} (E - E_b) d\xi = -\frac{(u_b - u_a)^2}{4} \pi\varepsilon \sqrt{\frac{1}{2(\gamma+1)}}. \tag{A6}$$

Appendix B. The Godunov methods in Lagrangian coordinate

We briefly introduce the Godunov methods with the exact Riemann solver for the adiabatic equation in this paper.

B.1. The representation of a Riemann solver in Lagrangian coordinate

1. Solve the exact Riemann problem with initial data $U_j = (\tau_j, u_j, E_j)$ and $U_{j+1} = (\tau_{j+1}, u_{j+1}, E_{j+1})$. Now we obtain the solutions U_L^* and U_R^* in star region, i.e., $u^*,\ P^*,\ \rho_L^*,\ c_L^*,\ E_L^*,\ \rho_R^*,\ c_R^*,\ E_R^*$.
2. If the left wave is shock $P^* > P_j$, then the signal velocity is shock velocity in Lagrangian coordinate,

$$s_{j+1/2}^1 = -\rho_j c_j \sqrt{\frac{\gamma+1}{2\gamma}\frac{P^*}{P_j} + \frac{\gamma-1}{2\gamma}}.$$

If the left wave is rarefaction wave $P^* < P_j$, then speeds of rarefaction wave head and tail are $\lambda_l^1 = -\rho_j c_j$, $\lambda_r^1 = -\rho_L^* c_L^*$, respectively, and the characteristic velocity is

$$s_{j+1/2}^1 = 0.5(\lambda_l^1 + \lambda_r^1).$$

For both shock and rarefaction wave, the left wave jump is

$$W_{j+1/2}^1 = U_L^* - U_j = (\tau_L^* - \tau_j, u^* - u_j, E_L^* - E_j).$$

3. The contact wave speed is zero, i.e., $s_{j+1/2}^2 = 0$, and the wave jump is

$$W_{j+1/2}^2 = U_R^* - U_L^* = (\tau_R^* - \tau_L^*, 0, E_R^* - E_L^*).$$

4. If the right wave is shock $P^* > P_{j+1}$, then the signal velocity is

$$s_{j+1/2}^3 = \rho_{j+1} c_{j+1} \sqrt{\frac{\gamma+1}{2\gamma}\frac{P^*}{P_{j+1}} + \frac{\gamma-1}{2\gamma}}.$$

If the right wave is rarefaction wave $P^* < P_{j+1}$, then speeds of rarefaction wave head and tail are $\lambda_r^3 = \rho_{j+1} c_{j+1}, \lambda_l^3 = \rho_R^* c_R^*$, respectively, and the characteristic velocity is defined by

$$s_{j+1/2}^3 = 0.5(\lambda_l^3 + \lambda_r^3).$$

For both of the cases, the right wave jump is

$$W_{j+1/2}^3 = U_{j+1} - U_R^* = (\tau_{j+1} - \tau_R^*, u_{j+1} - u^*, E_{j+1} - E_R^*).$$

B.2. The wave jump in HLL type Riemann solver

The star region is

$$U^H_{j+\frac{1}{2}} = \frac{s^3_{j+1/2}U_{j+1} - s^1_{j+1/2}U_j + F_j - F_{j+1}}{s^3_{j+1/2} - s^1_{j+1/2}}.$$

The wave jump is

$$W^H_{j+1/2} = \left(U^H_{j+\frac{1}{2}} - U_j, 0, U_{j+1} - U^H_{j+\frac{1}{2}}\right)^T.$$

B.3. The Godunov method in Lagrangian formulation

For a given domain $[0,L]$ and an initial mesh size Δx^0_j, we first set the initial conditions $U^0_j = (\tau^0_j, u^0_j, E^0_j)$ at time $t = 0$. The mass in each cell $\Delta\xi_j = \rho^0_j \Delta x^0_j$. Then, for each time step n, we perform the following operations:

Step(I): Boundary conditions. This is carried out by adding some ghost cells, just like traditional Euler method.

Step(II): Solution of Riemann problem. For each pair of data states U^n_j and U^n_{j+1}, compute the solution of Riemann problem and compute: particle velocity and pressure $u^*,\ P^*$, wave speeds $s^p_{j+1/2}$, and wave jumps $W^p_{j+1/2},\ p = 1,2,3$, see previous B1 part for detail.

Step(III): Computation of time step,

$$\Delta t \leqslant C_{cfl}\frac{\Delta\xi_j}{\max_j\left(-s^1_{j+1/2}, s^3_{j+1/2}\right)},$$

where a choice of C_{cfl} is made at the beginning of the computations.

Step(IV): Computation of flux $F = (-u, P, Pu)$. For the first order Godunov method,

$$F^{G1}_{j+1/2} = (-u^*, P^*, P^*u^*)^T. \tag{B1}$$

For the first order HLL type method,

$$F^{H1}_{j+\frac{1}{2}} = \frac{s^3_{j+1/2}F_j - s^1_{j+1/2}F_{j+1} + s^1_{j+1/2}s^3_{j+1/2}(U_{j+1} - U_j)}{s^3_{j+1/2} - s^1_{j+1/2}}. \tag{B2}$$

For the second order Godunov method,

$$F^{G2}_{j+1/2} = F^{G1}_{j+1/2} + \frac{1}{2}\sum_{p=1}^{3}\left|s^p_{j+1/2}\right|\left(1 - \frac{\Delta t}{\Delta\xi_j}\left|s^p_{j+1/2}\right|\right)\widetilde{W}^p_{j+1/2}. \tag{B3}$$

where $\widetilde{W}^p_{j+1/2}$ is a limited version wave $W^p_{j+1/2}$, see (34)–(36).For the second order HLL type method,

$$F^{H2}_{j+1/2} = F^{H1}_{j+1/2} + \frac{1}{2}\sum_{p=1}^{3}\left|s^p_{j+1/2}\right|\left(1 - \frac{\Delta t}{\Delta\xi}\left|s^p_{j+1/2}\right|\right)\widetilde{W}^{H,p}_{j+1/2}, \tag{B4}$$

where the definition of a limited version $\widetilde{W}^H_{j+1/2}$ is the same as (34)–(36).For the second order Hybrid method

$$F^{HYB,1}_{j+1/2} = F^{G2,1}_{j+1/2}, \quad F^{HYB,2}_{j+1/2} = F^{G2,2}_{j+1/2}, \quad F^{HYB,3}_{j+1/2} = F^{H2,3}_{j+1/2}. \tag{B5}$$

Step(V): Computation of new grid position.

$$x^{n+1}_{j+1/2} = x^n_{j+1/2} - \Delta t F^1_{j+1/2}.$$

Step(VI): Updating of solution.

$$U^{n+1}_j = U^n_j + \frac{\Delta t}{\Delta\xi}\left(F_{j+1/2} - F_{j-1/2}\right).$$

To keep geometrical conservation, we update the density as

$$\rho^{n+1}_j = \Delta\xi / \left(x^{n+1}_{j+1/2} - x^{n+1}_{j-1/2}\right).$$

Step(VII): Next time level. Go to (I).

References

[1] J. Von Neumann, R.D. Richtmyer, A method for the numerical calculation of hydrodynamic shocks, J. Appl. Phys. 21 (1950) 232–237.
[2] S.K. Godunov, A difference method for numerical calculation of discontinuous solutions of the equations of hydrodynamics, Mat. Sb. 47 (1959) 271–306.
[3] J. Quirk, A contribution to the great Riemann solver debate, Int. J. Numer. Meth. Fluids 18 (1994) 555–574.
[4] T.W. Roberts, The behavior of flux difference splitting schemes near slowly moving shock waves, J. Comput. Phys. 90 (1990) 141–160.
[5] S. Jin, J.G. Liu, The effects of numerical viscosities I. Slowly moving shocks, J. Comput. Phys. 126 (1996) 373–389.
[6] S. Karni, S. Canic, Computations of slowly moving shocks, J. Comput. Phys. 136 (1997) 132–139.
[7] M. Arora, P. Roe, On post-shock oscillations due to shock capturing schemes in unsteady flows, J. Comput. Phys. 130 (1997) 25–40.
[8] K. Xu, J. Hu, Projection dynamics in Godunov-type schemes, J. Comput. Phys. 142 (2) (1998) 412–427.
[9] R.E. Peierls, Theory on von Neumann's Method of Treating Shocks, Technical Report LA-332, Los Alamos Scientific Laboratory, 1945.
[10] W.F. Noh, Errors for calculations of strong shocks using an artificial viscosity and an artificial heat flux, J. Comput. Phys. 72 (1987) 78–120.
[11] R. Menikoff, Errors when shock-waves interact due to numerical shock width, SIAM J. Sci. Comput. 15 (1994) 1227–1242.
[12] M. Gehmeyr, B. Cheng, D. Mihalas, Noh's constant-velocity shock problem revisited, Shock Waves 7 (1997) 255–274.
[13] W.J. Rider, Revisiting wall heating, J. Comput. Phys. 162 (2000) 395–410.
[14] W.H. Hui, S. Kudriakov, On wall overheating and other computational difficultes of shock-capturing methods, Comput. Fluid Dyn. J. 10 (2) (2001) 192–209.
[15] R.P. Fedkiw, A. Marquina, B. Merriman, An isobaric fix for the overheating problem in multimaterial compressible flows, J. Comput. Phys. 148 (1999) 545–578.
[16] A. Harten, P.D. Lax, B. van Leer, On upstream differencing and Godunov-type schemes for hyperbolic conservation laws, SIAM Rev. 25 (1) (1983) 35–61.
[17] M. Shashkov, Conservative Finite Difference Method on General Grids, CRC Press, Boca Raton, FL, 1996.
[18] R. Landshoff, A numerical method for treating fluid flow in the presence of shocks, LASL Rept. No. LA-1930, Los Alamos, New Mexico, 1955.
[19] W.J. Rider, A review of approximate Riemann solvers with Godunov's method in Lagrangian coordinates, Comput. Fluids 23 (2) (1994) 397–413.
[20] H.S. Shui, Difference Methods for One Dimension Hydrodynamic Fluids Problems, Defence Industry Press, Beijing, 1998 (in Chinese).
[21] E.F. Toro, Riemann Solvers and Numerical Methods for Fluid Dynamics, Springer-Verlag, Berlin, New York, 1997.
[22] P.L. Roe, Approximate Riemann solvers, parameter vectors, and difference schemes, J. Comput. Phys. 43 (1981) 357–372.
[23] E.F. Toro, M. Spruce, W. Speares, Restoration of the contact surface in the HLL-Riemann solver, Shock Waves 4 (1994) 25–34.
[24] D. Hoff, T.P. Liu, The inviscid limit for the Navier–Stokes equations of compressible, isentropic flow with shock data, Indiana Univ. Math. J. 38 (4) (1989) 861–915.
[25] W.J. Rider, An adaptive Riemann solver using a two-shock approximation, Comput. Fluids 28 (1999) 741–777.
[26] B. Einfeldt, C.D. Munz, P.L. Roe, B. Sjogreen, On Godunov-type methods near low densities, J. Comput. Phys. 92 (1991) 273–295.
[27] J. Glimm, Solution in the large for nonlinear hyperbolic systems of equations, Commun. Pure Appl. Math. 18 (1965) 697–715.
[28] A.J. Chorin, Random choice solutions of hyperbolic systems, J. Comput. Phys. 22 (1976) 517–533.
[29] P. Colella, An Analysis of the Effect of Operator Splitting and of the Sampling Procedure on the Accuracy of Glimms Method, Ph.D. Thesis, Department of Mathematics, University of California, USA, 1978.
[30] P. Colella, Glimms method for gas dynamics, SIAM J. Sci. Stat. Comput. 3 (1) (1982) 76–110.
[31] G.A. Sod, A numerical study of a converging cylindrical shock, J. Fluid Mech. 83 (1977) 785–794.
[32] A. Harten, M. Hyman, Self adjusting grid methods for one-dimensional hyperbolic conservation laws, J. Comput. Phys. 50 (1983) 235–269.
[33] R. Leveque, Finite Volume Methods for Hyperbolic Problems, Cambridge Univeristy Press, Cambridge, 2002.
[34] S. Osher, S. Chakravarthy, High resolution schemes and the entropy condition, SIAM J. Numer. Anal. 21 (5) (1984) 955–984.
[35] C. Shu, S. Osher, Efficient implementation of essentially non-oscillatory shock-capturing schemes II, J. Comput. Phys. 83 (1988) 32–78.
[36] C.W. Shu, TVB boundary treatment for numerical solutions of conservation laws, Math. Comput. 49 (1987) 123–134.
[37] A. Marquina, Local piecewise hyperbolic reconstruction of numerical fluxes for nonlinear scalar conservation laws, SIAM J. Sci. Comput. 15 (4) (1994) 892–915.
[38] R. Donat, A. Marquina, Capturing shock reflections: an improved flux formula, J. Comput. Phys. 125 (1996) 42–58.
[39] G.A. Sod, A survey of several finite difference methods for systems of nonlinear hyperbolic conservation laws, J. Comput. Phys. 27 (1978) 1–31.
[40] R.D. Richtmyer, K.W. Morton, Difference Methods for Initial Value Problems, Wiley-Interscience, New York, 1967.